JOURNAL OF CATALYSIS 75, 175–184 (1982)

Ferromagnetic-Resonance Investigation of the Nickel/Graphite–Hydrogen System

A. J. SIMOENS, E. G. DEROUANE,[1] AND R. T. K. BAKER

Corporate Research-Science Laboratories, Exxon Research and Engineering Company, Linden, New Jersey 07036

Received August 26, 1981; revised January 1, 1982

Catalytic channels created by nickel particles during the hydrogenation of graphite cease at around 1250 K as the metal spreads and wets the sides of the channels with a resultant loss in activity. Particles are reformed along the edges of the channels by subsequent reaction in steam at 1125 K. In an attempt to learn more about this extraordinary behavior of nickel, both in the wetted and redispersed states we investigated the ferromagnetic properties of the nickel–graphite system treated under various conditions. Ferromagnetic resonance (FMR) provides both qualitative and quantitative information on particle size and shape, degree of reduction, surface anisotropy, and metal–support constraints for the dispersed ferromagnetic metal. In addition to confirming many of the previous conclusions on this system, the FMR data point to the existence of a strong nickel–graphite interaction which is broken by treatment in steam.

INTRODUCTION

Previous studies using controlled atmosphere electron microscopy (CAEM) (*1, 2*) and chemisorption techniques (*3*) revealed that at temperatures near 1250 K, nickel on graphite was undergoing dramatic changes. The catalytic channels created by the nickel particles moving across the surface of graphite in H_2 ceased. This deactivation was believed to be associated with the presence of a strong nickel–carbon interaction, causing the metal to spread and wet the interior of the channels as a near monolayer (*3*) with a resultant loss in catalytic activity (*2*). Reheating deactivated samples in O_2 or H_2O resulted in the formation of smaller discrete particles along the sides of the channels, the latter showing again catalytic activity in the presence of hydrogen (*2*).

No direct evidence was, however, provided for the nature of the nickel–carbon interaction. The thin film form of nickel in the wetted (deactivated) state was eventually inferred from model calculations describing the progressive depletion of the nickel particles in the propagating channels (*3*).

In an attempt to learn more about this extraordinary behavior of nickel, both in the wetted and redispersed states, it was decided to investigate the ferromagnetic properties of the Ni–grafoil system, treated under various conditions. Ferromagnetic resonance (FMR) was used as it was shown to provide qualitative and quantitative information on particle size and shape, degree of reduction, surface anisotropy, and metal–support constraints for the dispersed ferromagnetic metal (*4–5*).

EXPERIMENTAL

Catalyst

As single-crystal graphite, used in the CAEM studies (*1, 2*), was not in sufficient supply for bulk experiments, grafoil (Union Carbide, lot 63509, GTA grade) was selected as the carbonaceous material. A nickel on grafoil catalyst was prepared by incipient wetness impregnation of grafoil chips with an aqueous solution of nickel acetate (Matheson CB 530). The catalyst was thoroughly mixed for 0.5 h, and dried

[1] On leave from Facultes Universitaires de Namur, Department of Chemistry, Namur, Belgium.

0021-9517/82/050175-10$02.00/0

at 400 K overnight. The procedure was repeated once leading to a Ni–grafoil catalyst containing about 5 wt% of nickel.

The catalyst was reduced at about 875 K for 2 h in a mixture of H_2 (24 liters · h^{-1}) and He (6 liters · h^{-1}) and eventually passivated by passing an O_2 (1%)–He mixture over the catalyst for 0.5 h at room temperature and atmospheric pressure.

Ferromagnetic Resonance (FMR) Studies

The dynamic or *in situ* investigations reported here were performed with a Bruker BER-420 electron paramagnetic resonance spectrometer operating in the *X* band. First derivative spectra were obtained by scanning the magnetic field between 0 and 10 kOe and using a modulation frequency of 100 kHz. The spectrometer was equipped with a conventional rectangular TE_{102}-cavity fitted with a variable temperature unit (up to 625 K) or with a cylindrical, water-cooled, high-temperature (up to 1275 K) cavity. In both cases, the sample temperature was varied by adjusting the temperature of a dry nitrogen stream flowing around the EPR microreactor. It was measured by a thermocouple located near the bottom of the microreactor, referring in addition to a calibration curve to account for possible temperature gradients between the inside and the outside of the EPR cell. The EPR quartz microreactor containing the catalyst sample is schematized in Fig. 1. It allows *in situ* pretreatment of the sample in various conditions, including eventual catalytic reactions.

In order to permit quantitative measurements (for line intensities, line positions, or lineshapes) particular care was attached to avoiding changes in the EPR cavity quality factor, Q, as a function of temperature or at resonance (due to the extremely high magnetic susceptibility of ferromagnetic samples).

The following section describe the type of information provided by ferromagnetic resonance and the manner by which it is derived from the experimental data.

1. FMR Line Intensity

The line intensity I, is proportional to the magnetization of the sample. It is either ideally determined by double integration of the first derivative of the absorption curve, or relatively from Eq. (1);

$$I = \alpha \cdot y' \cdot \Delta H_{pp}^2, \qquad (1)$$

where y' is the first-derivative line amplitude, and ΔH_{pp} is the peak-to-peak linewidth, α is a proportionality factor which will depend solely on the lineshape.

The magnetization of small particles, M, will be equal to the product of the spontaneous magnetization, M_s and the Langevin function, L (*6*). When the sample is ferromagnetic, $L = 1$ and the FMR line intensity will vary as M_s: for nickel, it remains almost constant from 0 to 450 K, and then drops very rapidly near the Curie temperature (631 K).

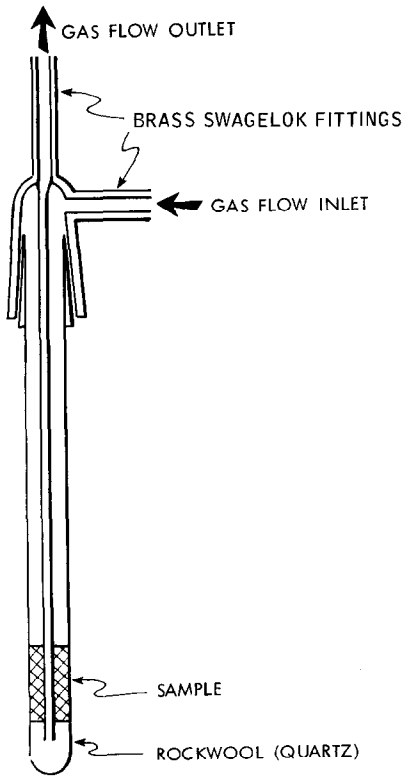

FIG. 1. EPR/FMR *in situ* microreactor cell.

Small particles become superparamagnetic if their magnetic relaxation time is smaller than the measuring time (for FMR, 10^{-10} sec). In order to attain this condition, the magnetic anisotropy energy has to be negligible. The Langevin function will then affect the shape of the M versus T plot. For extreme conditions (very small particles and high temperatures), the FMR line intensity will vary as T^{-1}.

The classical method to measure the Curie temperature, T_c, is to plot the magnetization, M, versus temperature, and determine the point where M disappears. However, above T_c ferromagnetic samples behave as paramagnets and in the magnetic field employed in FMR (~3000 Oe) their magnetization is not negligible resulting in an overestimated T_c value.

This situation can be avoided by plotting the square of the magnetization as a function of temperature. Such a plot will be linear over a temperature range of $0.9 < T/T_c < 1.0$.

The value of T_c (631 K for bulk nickel) will be affected by the particle size when the particles are incompletely reduced (*4*, *5*). Alloying the metal with impurities or other nonferromagnetic metals will decrease T_c dramatically (*7*). A strong metal–support interaction could also result in a drop of Curie temperature, but this decrease has never actually been observed to be greater than 40 K for completely reduced particles. In one case, Ni/SiO_2, T_c was observed to be increased by 15 K above the bulk Curie temperature (*4*).

2. Lineshape

The general resonance condition for a single ferromagnetic crystallite is given by Eq. (2) (*8*):

$$\frac{h\nu}{g\beta} = ((H_o + H_{axz})(H_o + H_{ayz}))^{1/2}, \quad (2)$$

where h is Planck's constant, ν the fixed microwave frequency, β Bohr's magneton, and g is a proportionality constant called the g factor (2.22 for nickel). The resonance condition is fulfilled when the applied static magnetic field **H** is equal to the resonance field H_o. H_{axz} represents the difference between the magnetic anisotropy fields along the ox and oz axis, where ox represents the direction of the radiofrequency field and oz the direction of **H**.

The most important magnetic anisotropies are briefly described under the next four headings:

(a) The shape anisotropy shifts the absorption line to lower fields when the particle is oriented with its longest axis along **H**. The shape anisotropy will be proportional to the spontaneous magnetization and will not be affected by the particle size or by chemisorption. The value of the shape anisotropy field will depend on the particle shape and can only be calculated for simple geometrical shapes (*9*). We will, therefore, consider the particles to be ideally ellipsoid of revolution. The measured value of the anisotropy field will then allow us to calculate a relative value of the ratio of the revolution axis, c, to the equatorial axis, a.

(b) The magnetocrystalline anisotropy of nickel is weak when compared to that of other ferro- or ferrimagnetic materials. Indeed, it was not detected for small supported crystallites of nickel (*4*) and the question can be asked if this is due to the small size of the crystallites (and consequently weak crystallinity) or to the presence of stronger anisotropies that override the magnetocrystalline anisotropy. In larger crystals, however, the resonance field is expected to be lowered when **H** is oriented along the (111) axis, increased along the (100) axis and slightly decreased along the (110) axis. The anisotropy is proportional in amplitude to K_1/M_s (where K_1 is the first-order magnetocrystalline anisotropy constant (*6*).

(c) The magnetostriction anisotropy (*6*) is proportional to the stress applied to the particles and to a proportionality factor $3\lambda/M_s$ (where λ is the magnetostriction coefficient). It allows us to estimate the strength of the metal–support interaction. The reso-

nance line will be shifted to lower fields when the compressed axis is oriented along the external static field.

(d) A series of magnetic anisotropies are typical of small supported metal crystallites, such as the *exchange anisotropy* between the metal and the support (*10*), *the magnetostriction anisotropy* arising from *surface tensions* (*11*), *Néel's surface anisotropy* (*12*), and the *interaction anisotropy* arising from dipole–dipole couplings between neighboring particles. These interactions are not well evaluated at the present time. It is known, however, that they will be dependent on the particle size and/or on the gas environment (chemisorbed species).

In a real catalyst the value and orientation of the magnetic anisotropies will change from particle to particle. The net effect on the line is described below.

(i) If no anisotropies are present, the line is about 300 Oe wide with a Lorentzian shape.

(ii) A small anisotropy will increase the width of the Lorentzian line, and gradually change it into Gaussian shape. This line will be slightly asymmetrical and the anisotropy field, H_a can be measured by (*13*)

$$H_a = \alpha(\Delta H_{pp} - 300), \qquad (3)$$

where α depends on the lineshape (Lorentzian = 1.7321, Gaussian = 1.1776).

(iii) If the anisotropy values are much larger than 300 Oe, and do not change from one crystallite to another, the line will appear as a powder spectrum with either a uniaxial (*4*) or cubic angular distribution (*14*), as in an EPR powder spectrum. This line is then very asymmetrical and the positions of the maximum and minimum of the first derivative of the absorption line allows the determination of the values of the anisotropy field.

(iv) If a broad range of anisotropy values is present, the angular distribution will be broadened and smeared out into a large Gaussian-type line.

RESULTS AND DISCUSSION

Reaction conditions are summarized in Table 1. They were chosen inasmuch as possible to reproduce standard CAEM and chemisorption treatments as previously described (*2, 3*). Figure 2 shows relative variations of FMR signal intensity with pretreatments while Figs. 3 and 4 report the

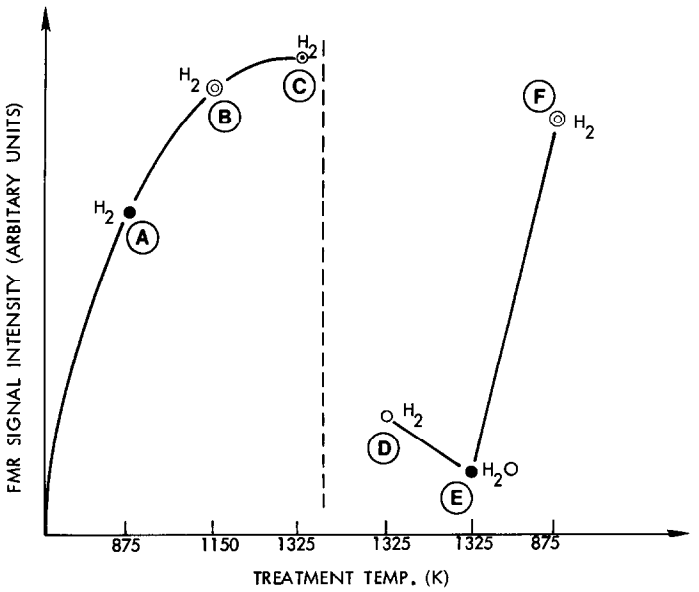

FIG. 2. Variation of FMR signal intensity at 473 K as a function of pretreatment (see Table 1).

TABLE 1

Reaction Conditions for the FMR Investigations on Nickel/Grafoil

Pre treatment	Temperature (K)	Time (h)	Gas environment
A	875	1.0	H_2 (9 liter · h^{-1})
B	1150	0.5	H_2 (9 liter · h^{-1})
C	1325	0.5	H_2 (9 liter · h^{-1})
D	1325	1.5	H_2 (9 liter · h^{-1})
E	1325	1.0	H_2O : He (1 : 40; 6 liter · h^{-1})
F	875	1.0	H_2 (9 liter · h^{-1})

Note. A = Re-reduction of Ni/grafoil. B = Onset of C gasification. C–D = Ni wetting and spreading. E = Breaking of Ni–C interaction. F = Redispersion of catalyst, re-reduction.

corresponding thermomagnetic curves in the temperature range 395–625 K.

Observed linewidths following the different treatments are plotted in Fig. 5 as a function of temperature. Lineshapes are also characterized by the line amplitude asymmetries plotted in Figs. 6 and 7 as W/W' vs measurement temperature, W and W' being evaluated as described here below:

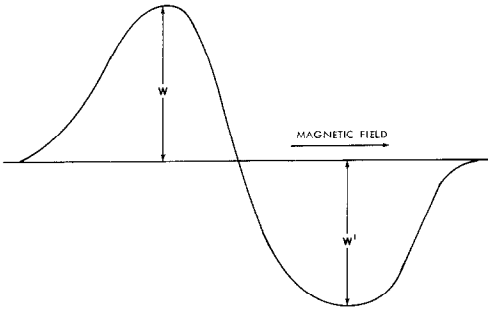

Values in Fig. 2 are only indicative when they are compared at a fixed temperature. They indeed depend intimately on the shape of the thermomagnetic curve which is different for ferromagnetic monodomains or polydomains, and for superparamagnets.

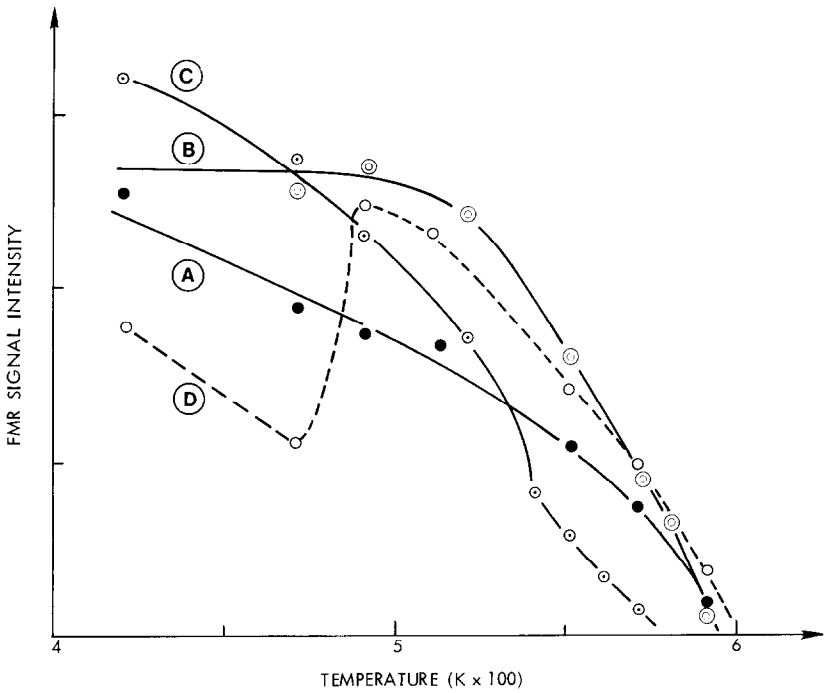

FIG. 3. Thermomagnetic curves following various pretreatments (A) to (D), see Table 1. FMR intensity values were calculated from Eq. (1) assuming $\alpha = 1$.

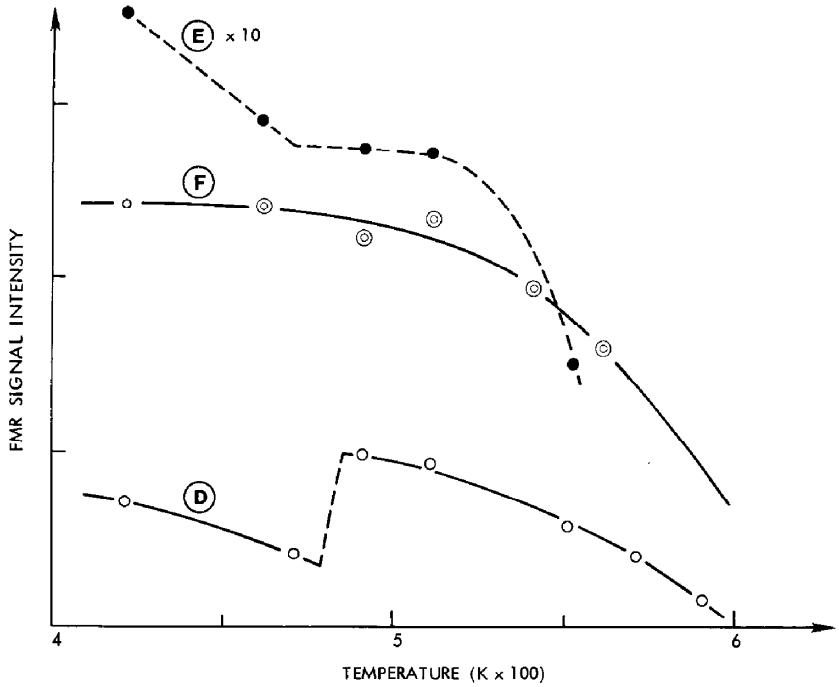

FIG. 4. Thermomagnetic curves following various pretreatments (D) to (F), see Table 1. FMR intensity values were calculated from Eq. (1) assuming $\alpha = 1$.

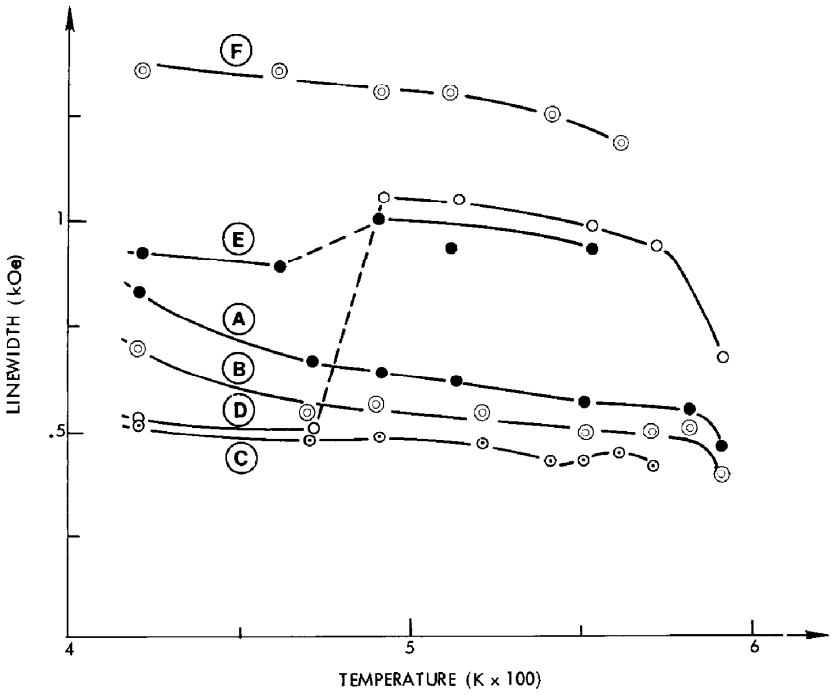

FIG. 5. FMR linewidths (kOe) as functions of measurement temperature following the pretreatments described in Table 1.

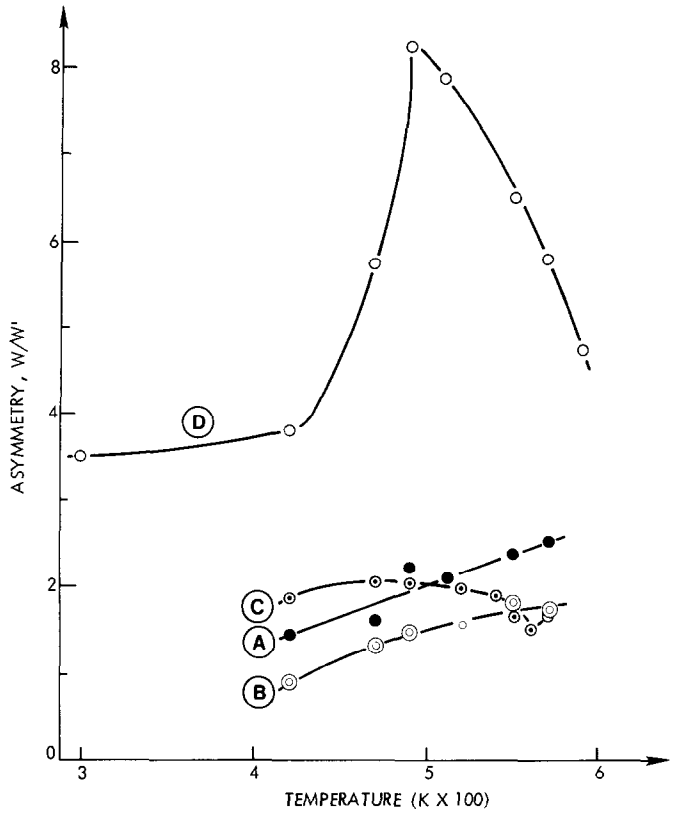

FIG. 6. Line amplitude asymmetry (W/W') as a function of measurement temperature for various pretreatments (A) to (D), see Table 1.

The thermomagnetic curve is shifted in addition along the temperature scale if T_c varies. Nevertheless, it is clear that prereduction at 875–1150 K (A) and (B) maximizes the amount of metallic nickel, that part of the Ni is removed from detection when spreading and wetting occurs (D), that treatment by steam further reduces the observable amount of ferromagnetic Ni (E) and that re-reduction (regeneration) in H_2 (F) restores nearly the original FMR intensity, i.e., the amount of metallic nickel.

It is observed that treatments in hydrogen at 875–1150 K (A and B) results in particle growth. Indeed the curve shapes in Fig. 3 indicate that particles change from a superparamagnetic to a ferromagnetic state. The linewidths vary roughly as the spontaneous magnetization (with the exception of the lowest temperature point) revealing the presence of a small shape anisotropy. The positive value of the line amplitude asymmetry indicates that the shape anisotropy is due to slightly flattened particles. The decrease of linewidth when going from (A) to (B) shows that the particles are becoming more spherical in shape at higher temperatures.

Two states of nickel (bidispersion) are observed after treatment in hydrogen at 1325 K (C) to (E) as shown by abrupt variations in the thermomagnetic plots of Figs. 3 to 7. One state is characterized by a Curie temperature well below that of pure and bulk nickel (631 K): 540 K for treatment (C) and 480 K for treatments (D) and (E). The second nickel state has a Curie point which is only slightly shifted (580–600 K). A Curie temperature shift of about 30 K is typically what would be expected for small particles

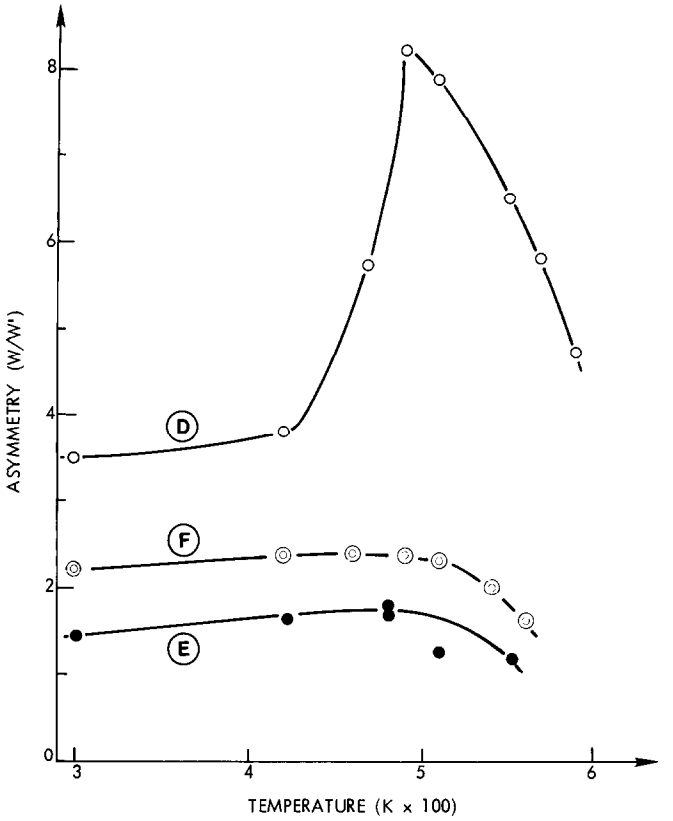

FIG. 7. Line amplitude asymmetry (W/W') as a function of measurement temperature for various pretreatments (D) to (F), see Table 1.

interacting with a support, while larger shifts (in this case 150 K) may be associated with incomplete reduction or alloying effects (*4*, *5*). It is also clear that the original sample (A) or the redispersed catalyst (F) have near normal Curie points indicating weak metal–support interactions and near complete reduction.

The higher linewidth and the very high line amplitude anisotropy of the ferromagnetic phase having a Curie point of near 600 K (D), as well as the temperature dependence of the linewidth, point out the existence of a very large shape anisotropy such as that encountered for film-like or plate-like particle shapes. From the positions of the maximum and minimum of this very asymmetrical line it is possible to calculate a c/a value of 1.05. However, this value is completely misleading as it is known from the microscopy data that the nickel film should have three very different axis lengths (~2500 : 50 : 1) and are thus not reducible to an ellipsoid of revolution.

As seen from Fig. 7, treatment in a H_2O–He environment suppressed the strong shape anisotropy (E), hence more spherical particles are regained by treatment in steam. Further treatment in hydrogen (F) shows indeed redispersion of Ni as much smaller and slightly flattened particles as evidenced by the high linewidth (Fig. 5) and an asymmetry factor of 2 (Fig. 7).

CONCLUSIONS

A synthesis of our observations and their interpretation is presented in Table 2. FMR information is completely consistent with the CAEM observations which indicate that

TABLE 2

FMR Data and Conclusions Regarding the Nickel/Graphite–Hydrogen System

(A) 875 K, H_2, 1 h	Ni particles are slightly flat and have near normal Curie temperature.
(B) 1150 K, H_2, 0.5 h	Particles are less flat; they have probably sintered as size has increased.
(C) 1325 K, H_2, 0.5 h	Bidispersion is apparent as two Curie points are observed. At this temperature, Ni depletion occurs.
(D) 1325 K, H_2, 1.5 h	Bidispersion is even more apparent. The film-like Ni phase interacts with graphite while the more globular Ni particles contain dissolved carbon.
(E) 1325 K, H_2O–He, 1 h	A bidispersion still exists but all particles are now spherical. The film-like structure has disappeared; part of the Ni has been oxidized.
(F) 875 K, H_2, 1 h	The original FMR intensity is restored; all the Ni is then recovered as metal; Ni particles are now smaller than originally and somehow flattened.

high-temperature treatment of Ni/graphite in hydrogen causes bidispersion as result of spreading of the catalytically active nickel particles. In addition, FMR shows or confirms that:

(a) The spread or film-like nickel has a near bulk Curie temperature; however, the small Curie temperature shift that is observed (30–50 K) could indicate the presence of a nickel–graphite interaction.

(b) Nickel does indeed wet and spread on the graphite support.

(c) Channeling Ni particles, initially rather spherical in shape, progressively become more oblate; this observation is in agreement with the previous model (*3*) in which flattening of the channeling particle should of course occur when Ni depletion takes place, the width and depth of the channel staying nearly constant.

(d) Inactive nickel particles which remain immobile on the graphite basal plane contain a significant amount of dissolved carbon, as evidenced by the large shift (150 K) in Curie temperature. This finding is consistent with the observation of Keep *et al.* (*1*) that at high temperatures graphite platelets are formed on immobile nickel particles.

(e) Deactivated (spread) nickel can indeed be redispersed as small metallic particles by successive treatments in H_2O–He and H_2 atmospheres.

The question could be raised as to the reason why nickel wets and spreads in an irreversible manner at 1250 K, whilst it does not do so at lower temperatures. It is possible that the material actually spreading onto the walls of the channels is not pure nickel but carbidic nickel, having a higher surface tension. Upon cooling, the nickel carbide could decompose to form metallic and ferromagnetic nickel with a graphite monolayer coating. This "sandwich" model would thus explain the observed loss of catalytic activity and the decrease in hydrogen chemisorption capacity.

Nickel carbide (Ni_3C) is expected to melt at about 1595 K (*15*). This could indicate that the molten skin surround the particle soft core is at a temperature 345 K higher than the measurement temperature. In addition, this model predicts a minimum value of 3 for the number of nickel monolayers.

The latter value is in excellent agreement with that calculated from the CAEM experiments (*3*), i.e., 3.1, by supposing that de-

position of nickel only takes place on the channel walls (surface density of nickel left over by the particles = 57 atoms/nm^2, surface density of one monolayer of close-packed nickel atoms = 18.6 atoms/nm^2).

Further work is in progress using other surface techniques to ascertain the nature of nickel in the thin film form.

ACKNOWLEDGMENTS

The authors would like to acknowledge the help of M. Estadt in the samples preparation. E.G.D. thanks F.N.R.S. (Belgium) for financial support as a "Credit aux Chercheurs."

REFERENCES

1. Keep, C. W., Terry, S., and Wells, M., *J. Catal.* **66,** 451 (1980).
2. Baker, R. T. K., and Sherwood, R. D., *J. Catal.* **70,** 198 (1981).
3. Baker, R. T. K., Sherwood, R. D., and Derouane, E. G., *J. Catal.*, in press.
4. Simoens, A. J., Dr. Sc. Thesis, University of Namur, Belgium, 1980.
5. Derouane, E. G., Simoens, A. J., Colin, C., Martin, G. A., Dalmon, J. A., and Védrine, J. C., *J. Catal.* **52,** 50 (1978).
6. Herpin, A., "Théorie du magnétisme." 1968, Presses Universitaires de France, Paris.
7. Vonsovskii, S. V., "Magnetism." Wiley, Chichester, 1974.
8. Kittel, C., *Phys. Rev.* **70,** 281 (1948); *J. Phys. Radium* **12,** 149 (1951).
9. Osborn, J. A., *Phys. Rev.* **67,** 351 (1954).
10. Andra, W., and Danan, H., *Phys. Status Solidi A* **42,** 227 (1977).
11. Chopra, K. L., "Thin Film Phenomena," pp. 271, 272. McGraw-Hill, New York, 1969. Janssen, M. M. P., *J. Appl. Phys.* **41,** 385 (1970).
12. Néel, L., *J. Phys. Radium* **15,** 225 (1954).
13. Srivastava, C. M., Patni, M. J., and Narradikar, N. G., *J. Phys. (Orsay, Fr)* **38,** Cl-267 (1977).
14. Schlömann, E., *J. Phys. Chem. Solids* **6,** 257 (1958).
15. Hansen, M., "Constitution of Binary Alloys." McGraw-Hill, New York, 1958.